Numerical Investigation of Oil injection in Screw Compressors

Nausheen BASHA*, Ahmed KOVACEVIC and, Sham RANE

City, University of London,
London, UK
Nausheen.basha.1@city.ac.uk

* Corresponding Author

ABSTRACT

Oil injected screw compressors are commonly used in the industry. The position and amount of oil injection are determined experimentally or by heat balances with an assumption of uniform oil distribution in the compression chamber, which is not validated. This paper presents a study on the oil distribution within a screw compressor chamber using Computational Fluid Dynamics (CFD) with Volume of Fluid (VOF) multiphase model. Prerequisite for using CFD in screw compressors is a body fitted numerical mesh produced by software SCORG. The analysis was carried out on a newly designed screw compressor with a 4-5 lobe combination. It was found out that injecting the oil through two separate holes, one on each rotor has advantages compared to the injection through a single hole. The injection holes are conveniently positioned to ensure an even oil distribution within the compression chamber. If the same amount of oil is injected through the two separate holes instead of originally designed single hole, the maximum gas temperature within the chamber could be reduced by 30°-35°C leading to reduction in specific power by 1.8%. Techniques used in this study can improve the performance and efficiency of a wide range of screw compressors.

Keywords: Power Consumption, Screw Compressor, Cooling, CFD, Volume of Fluid.

Nomenclature

c_p	specific heat capacity	J/kg/K
d	port diameter	mm
F	external body forces	N
g	gravity	m/s^2
h	enthalpy	J
k	turbulent kinetic energy	m^2/s^2
$\dot{m}$	mass flow rate	kg/s
N	rotational speed	rpm
P	pressure	bar
PW	power	W
Q	volume flow rate of air	m^3/min
T	temperature	°C
t	time	s
v	velocity	m/s
w	specific power	W/m^3/min
y^+	non-dimensional wall distance	
z	number of lobes on the rotor	

Greek Symbols

α	volume fraction	
γ	specific heat ratio of air	
δ	thermal conductivity	W/mK
η	efficiency	

θ	male rotor angle	degrees
μ	dynamic viscosity	kg/ms
ρ	density	kg/m^3
τ	torque	Nm
ω	specific dissipation rate	m^2/s^3

Subscripts

air	air phase
ad	adiabatic
comp	compressor
dis	discharge
i	indicated
inlet	fluid domain inlet
m	male rotor
f	female rotor
oil	oil phase
out	fluid domain outlet
outlet	fluid boundary condition

Acronyms

CFD	Computational Fluid Dynamics
SST	Shear Stress Transport
UDF	User Defined Functions
UDND	User Defined Nodal Displacement
VOF	Volume of Fluid

1. INTRODUCTION

The U.S Energy Information Administration (EIA) has projected that by 2050, world energy usage will increase by nearly 50%. More than 50% of this is attributed to the industrial sector where it is predicted that it will reach about 315 quadrillion British thermal units (332 trillion kJ). Approximately 10% of industrial electricity consumption is attributed to compressed air systems, amounting to approximately 1.3 TWh or 470 kt CO_2 each year in the UK alone [1]. Twin-screw compressors are also very common in refrigeration and air-conditioning systems. Therefore, even a small improvement in compressor efficiency can make significant savings in energy and CO_2 emissions.

Twin-screw compressors are widely used for industrial compression, in which the injection of lubricating oil improves their efficiency and reliability significantly by sealing the gaps and cooling the compressed air [2]. However, too much oil reduces efficiency due to increased viscous drag, while too little can lead to poor lubrication and reduced reliability. Oil injected screw machines have been in use since the 1960s, but there are only a few publications on how to determine the optimum amount of oil and internal oil distribution.

Early analytical studies dedicated to optimising oil injection were carried out by Singh and Bowman in 1986 [3], who developed a mathematical model to evaluate the effect of oil droplet size. However, later studies by Stosic et al. [4], indicated that oil mass flow had a larger effect. All these studies were based on the assumption of overall heat transfer rates between the air and oil. Peng et al. studied the effect of oil to gas mass ratio at varying rotational speeds [5], and De Paepe et al. [6] investigated how this varied both with shaft speed and discharge pressure. These showed that an optimum quantity of oil exists for a compressor running at a specific operating condition but did not account for how it is distributed within the compression chamber. This only became possible through the development of Computational Fluid Dynamics (CFD) analysis of flow within these machines.

CFD analysis of flow within screw machines was not explored until the 2000s when a methodology to produce block-structured grids, for deforming domains, was derived by Kovacevic et al. [7] which later led to a method to generate a single domain mesh. This resulted in better solution accuracy for single-phase flow of air in oil-free compressors [8]. But two-phase flow in oil-injected machines still posed a great challenge due to the complex geometry of the rotors, the very thin clearance gaps, high-density ratios between the gas and the oil, and the smearing of the gas-oil

interface when the compressible gas and the incompressible oil exist in the same domain. Hence, some researchers modelled the flow characteristics in oil-injected screw machines without the oil phase [9].

Then, Rane et al., analysed the flow in an oil-injected compressor through an Eulerian-Eulerian multiphase approach, which allowed visualising the distribution of oil for the first time within the compression chamber [10]. Other authors used the same Eulerian-Eulerian approach for application in an oil-injected twin-screw expander, but these studies were not validated by experimental data [11][12]. Some authors used a VOF multiphase model such as this one in Pumplinx, but the geometrical parameters of this machine had to be simplified to achieve a stable running conditions [13]. The alternative is the Euler-Lagrange approach but it is not suitable for an oil-injected compressor as initial data on oil droplet sizes is not available, and the oil volume fraction loading is higher than 12% which is the limit specified by CFD vendors [14].

The authors of this paper investigated a typical oil-injected air compressor to compare the Euler-Euler approach with the homogeneous model. The good agreement with experimental data was obtained from that study [15]. They also compared multiphase models using Eulerian-Eulerian, Volume of Fluid (VOF), and Mixture models for an oil-injected compressor [16]. It was shown that both power and flow rate predictions from the VOF model were close to experimental data, and solutions with the VOF model required 25% less time than the full Eulerian-Eulerian model. Therefore, the VOF model was selected for further, more detailed studies.

CFD, with VOF modelling, enables oil flow within the compression chamber to be visualised, but, to date, this has not been confirmed by test results. Some studies on oil distribution in simple bearing chambers and rotary compressors using CFD have shown how to improve cooling and lubrication performance [17][18][19]. This did not include screw compressors, due to their more complex rotor geometry. Consequently, this study was carried out to estimate both oil and temperature distribution within a screw compressor compression chamber and how this affects its performance and compares the predicted results with the experimental test data.

Previous CFD studies in this area were limited to consideration of oil admission through a single injection point. This revealed that high temperatures exist in the compression domain even if the oil flow rate is increased by a factor of ten. Therefore, separate injection point to each rotor was considered in this study to determine if this would improve.

2. COMPUTATIONAL STUDY

2.1 Governing equations

Oil injected in a screw compressor domain undergoes topological changes. Oil is continuously accelerated in the clearances changing its flow from continuous to discrete. Accounting for these topology changes is impossible within a single macroscale model for a case as complicated as that of an oil-injected screw compressor.

In the present study, the two-phase simulations are performed using the Volume of Fluid (VOF) model developed by Hirt and Nichols[20]. The VOF model assumes that both oil and gas are Newtonian immiscible fluids. The assumption on immiscibility holds true for this study as air and oil are normally immiscible in a typical oil-injected air compressor. However, for applications which include compression of organic fluids, suitable assumptions need to be made when using the VOF model [21].

The VOF model tracks the interface between the air and oil phase by solving the conservation equation for the volume fraction of the oil phase, as shown in equation (1) [22]. In each cell, $\alpha_{oil} = 1$ represents pure oil phase and $\alpha_{oil} = 0$ represents pure air phase. If $0 < \alpha_{oil} < 1$ it means that air-oil interface exists in that cell. In that case, the volume fraction of the air phase can be determined by the constraint shown in equation (2).

$$\frac{1}{\rho_{oil}}(\frac{\partial(\alpha_{oil}\rho_{oil})}{\partial t} + \nabla.(\alpha_{oil}\rho_{oil}\vec{v}) = 0 \tag{1}$$

$$\alpha_{oil} + \alpha_{air} = 1 \tag{2}$$

In the VOF model, the flow variables are volume fraction averaged in each computational cell. For instance, equation (3) shows the density ρ of the air-oil two-phase flow. Similarly, viscosity and thermal conductivity are volume fraction averaged for an air-oil mixture. The enthalpy and temperature in a computational cell are mass fraction averaged.

They are unique for each phase in the mixture but could be shared depending on the methods used in a multiphase model to define an interface between the phases within a computational cell. This is based on the volume fraction of each fluid in the computational cell and the surrounding cells.

Density of the mixture:

$$\rho = \alpha_{air}\rho_{air} + \alpha_{oil}\rho_{oil} \tag{3}$$

These flow variables are then used in a single set of governing equations for continuity, momentum and energy as follows [22]:

Continuity:

$$\frac{\partial \rho}{\partial t} + \nabla.(\rho\vec{v}) = 0 \tag{4}$$

Momentum:

$$\frac{\partial}{\partial t}(\rho\vec{v}) + \nabla.(\rho\vec{v}\vec{v}) = -\nabla p + \nabla.[\mu(\nabla\vec{v} + \nabla\vec{v}^T)] + \rho\vec{g} + \vec{F} \tag{5}$$

The transient and convection terms are located on the left-hand side of equation (5), while the terms on the right-hand side describe the pressure gradient, stress-strain, gravity and external body forces.

Energy:

$$\frac{\partial}{\partial t}\sum_{k=1}^{n}(\alpha_k\rho_k\, h_k) + \nabla.\left(\alpha_k(\rho_k\overrightarrow{u_k}h_k - \delta\nabla T)\right) = 0 \tag{6}$$

Where *k* represents the air and oil phase.

2.2 Computational domain and mesh
The oil-injected compressor in this study had an 'N' rotor profile with 4/5 lobe combination. The configuration and dimensions of the compressor are shown in Table 1. The oil port position remains the same with respect to the male rotor angle rotation for both single and two injection points. The difference is on the rotor side of the oil port placement.

Table 1. Screw compressor geometric characteristics

Parameter	Value
Rotor profile	'N' silent
Rotor lobe combination	4/5
Rotor centre-distance [mm]	67.5
Male rotor outer diameter [mm]	98.8
Female rotor outer diameter [mm]	77.8
Rotor length [mm]	153.14
Male rotor wrap angle [degrees]	306.647
Built-in volume ratio	4.6
Oil port position with male rotor angle [degrees]	68.7

The compressor flow domain is divided into moving domain around the rotors and stationary sub-domains for ports, as shown in Figure 1a. The structured numerical mesh for the single moving subdomain around the male and female rotors consists of only hexahedral cells. The nominal size of the interlobe, radial and axial leakage gaps in the mesh was 50µm. Grids for the moving fluid domains around rotors were generated in several transverse planes using the in house software SCORG [23], which employs the algebraic transfinite interpolation, numerical smoothing and orthogonalisation with the background blocking technique as described in [24]–[26]. The 3D mesh is generated by assembling 2D grids from these transverse cross-sections. One of the transverse 2D grids is shown in Figure 1b. The meshes generated by this means are recorded in files for all rotor positions required to complete one interlobe rotation cycle. Each node in these files contains the node number and rotor coordinates in the global coordinate system. The rotor movement is obtained by importing coordinates from subsequent grid files, so that point numbers remain the

same while their position changes in space with time. The CFD software used in this study is ANSYS Fluent 19.0. In order to implement mesh movement in Fluent, it was necessary to develop User Defined Nodal Displacement (UDND) to allow for importing a new mesh for each time step and parallelisation on a number of computer processors as described in [25], [26] and [27].

The suction, discharge, and oil injection ports are stationary fluid domains. The suction port includes both radial and axial sections. In the first instance, the oil injection port was located only on the female rotor side of the casing. For the second part of this study, the oil is injected on both, the male and female rotor sides. Numerical meshes for the stationary domains are tetrahedral cells generated from ANSYS Mesher. Numerical meshes of subdomains are integrated by the use of General Grid Interfaces (GGI). The three-dimensional grid structure for the full domain with rotors represented by the first layer of numerical cells on the rotor surface is shown in Figure 1c.
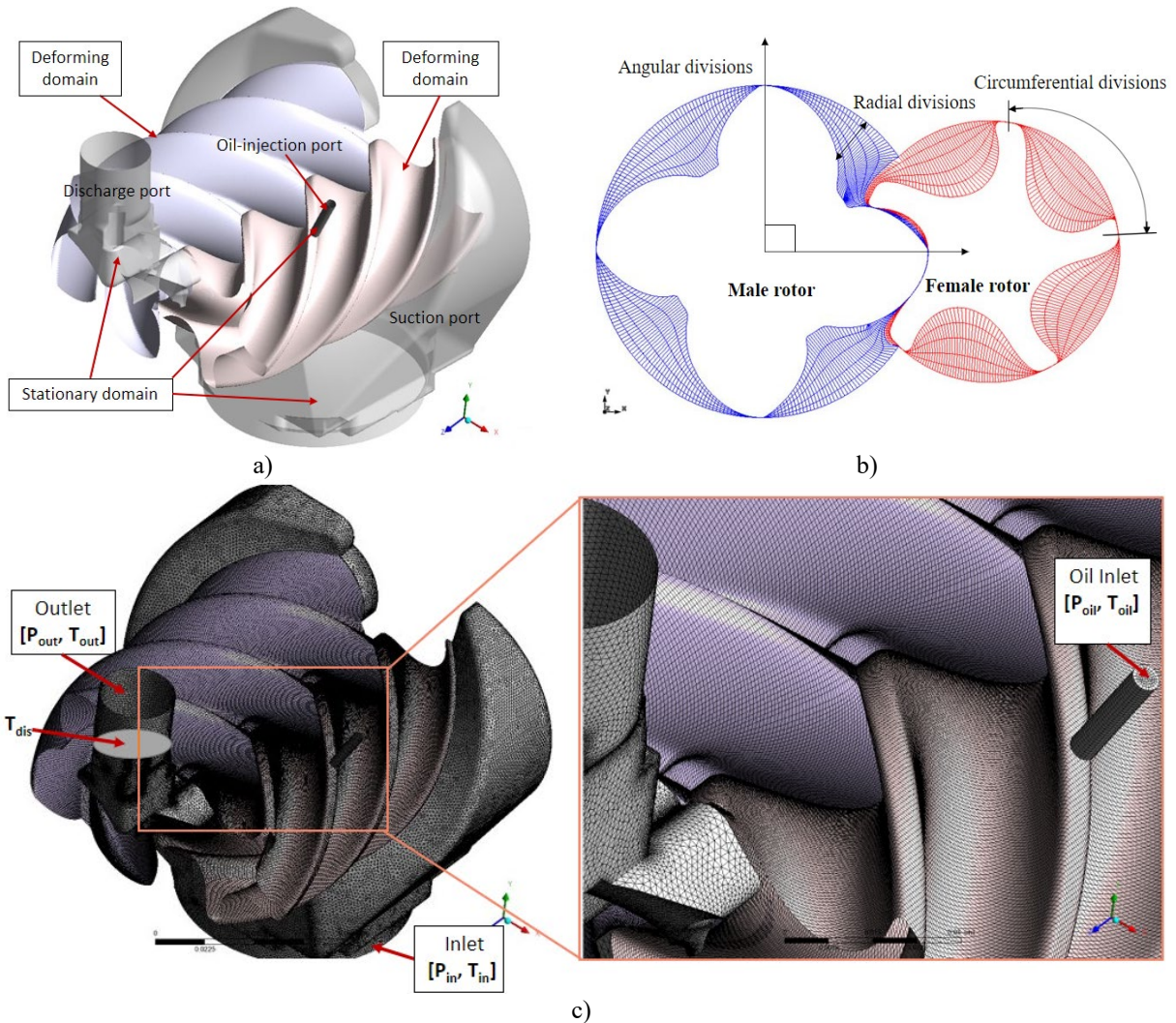

a)

b)

c)

Figure 1. (a) Computational domain of the compressor, (b) Rotor mesh in the transverse plane at 0° male rotor rotation and (c) Grid structure of the screw compressor

The rotor grids were generated with 60 circumferential division, 5 radial divisions, 90 angular divisions and 77 interlobe divisions that resulted in 924120 elements. The quality parameters of these grids are shown in Table 2. The best possible grid quality was obtained for the complex rotor domain though the quality was lower than the suggested practise. Therefore, the under-relaxation factors shown in Table 5 had to be used for achieving solution stability.

Table 2. Grid quality parameters

Parameters	Value	Best practice [30]
Maximum aspect ratio	326.0	<100.0
Maximum expansion factor	96.0	<20.0
Minimum orthogonal angle	6.9	>20.0

2.3   Case setup and preliminary results

The physical properties of air and oil are shown in Table 3. A coupled method is used for coupling the pressure and velocity fields with the value of flow courant number as 2. The inlet boundary condition is imposed with the fixed static pressure and specific temperature. For the outlet boundary, the static pressure and temperature are adopted. More details about the numerical setup are shown in Table 4.

y^+ in the domain was in the range of 0.5-62.0 and for this wide range of y^+ a hybrid turbulence model like SST k- ω was suitable. A transient analysis was carried out with a single time step of 2.778×10^{-05} s. The simulation was run for 0.051-0.083s, between 20-33 rotations of the male rotor depending upon the oil injection flow rate.

Table 3. Physical and thermal properties of air and oil phase

Property	Air	Oil
Fluid type	Ideal gas	Constant ρ 950 kg/m^3
c_p [J/kg/K]	1004.4	1800
μ [kg/ms]	1.831×10^{-5}	0.08
δ [W/mK]	2.61×10^{-2}	0.18

Table 4. Numerical simulation settings with FLUENT

Parameters	Value	Parameters	Setting
Air inlet pressure, P_{in} [bar]	0	Gradient	Green-Gauss Node Based
Air inlet temperature, T_{in} [°C]	27	Volume Fraction	Compressive
Oil inlet pressure, P_{oil} [bar]	8.5/10.5	Turbulence Scheme	First-order upwind
Oil inlet temperature, T_{oil} [°C]	50	Energy	First-order upwind
Outlet pressure, P_{outlet} [bar]	8.5/10.5	Transient Scheme	First-order implicit
Heat flux for rotor, casing and port walls [W/m^2]	0	Iterations per time step	100
		Convergence Criteria	Continuity 0.001, Velocity 0.001, Energy 1e-06, Turbulence 0.001, Volume Fraction 0.001

Table 5. List of under-relaxation factors

Variable	Value
Momentum	0.75
Pressure	0.75
Density	1.00
Body forces	1.00
Volume fraction	0.50
Turbulent kinetic energy	0.80
Specific dissipation rate	0.80
Turbulent viscosity	1.00
Energy	0.90

Mesh independence test was conducted for the case study with the single oil injection port of 5mm diameter. The study included simulations on three different mesh sizes with the grid refinement ratio of 1.2. The summary of the results of this study is given in Table 6. The mass flow rate of air is regarded as an evaluation criterion calculated as an average of the mass flow rate of air at the inlet and outlet. The relative difference in the mass flow rate between grids 2 and 3 is 0.15%. Therefore, grid number 2, which consists of 924,120 elements, was used for further simulations with various case studies.

Table 6. Mesh independence study results

Grid number	Number of elements-rotors	Total elements (rotor+ports)	$\dot{m}_{air}$ (kg/s)	Relative deviation (%)
1	761940	1,500,214	0.0722	1.8%
2	924120	1,662,394	0.0736	-
3	1074060	1,812,334	0.0735	-0.15%

The overview of case studies for the given injection port diameters is given in Table 7. Similar to the calculation for the mass flow rate of air, the mass flow rate of oil is calculated as an average of inlet and outlet mass flow rate of oil.

Also, the resulting torque on each rotor can be calculated from the surface pressure, and the orientation and position of the rotor cell surface. The power due to the torque acting on the rotors can be considered as indicated power. This indicated power can then be calculated according to the equation (7). For this compressor design, $z_m = 4$ and $z_n = 5$.

To account for compressor power, 15% mechanical losses are added to this indicated power value.

$$PW_i = \frac{2\pi N (\tau_m + \frac{z_m}{z_n} \tau_g)}{60} \tag{7}$$

All case studies were carried out at a rotational speed of 6000 rpm.

Table 7. Simulated case studies

	Single oil injection port		
d_{oil} [mm]	$\dot{m}_{oil}/\dot{m}_{air}$	P_{out} [bar]	P_{oil} [bar]
3	1.6	8.5	8.5
	1.8	10.5	10.5
4	3.2	8.5	8.5
	3.8	10.5	10.5
5	5.3	8.5	8.5
	6.3	10.5	10.5
8	15.3	8.5	8.5
	17.4	10.5	10.5
	Two oil injection ports		
d_{oil1}= 3.5 and d_{oil2}= 3.6, equivalent d_{oil}= 5	5.3	8.5	8.5
	5.7	10.5	10.5

The cell-averaged discharge temperature (T_{dis}) obtained at a cross-section closer to the outlet with the progressing simulation time was used to check when the steady-state condition was achieved. Discharge temperature with the accumulated solution time is shown in Figure 2a for 8.5bar. For the 3mm oil injection port, nearly 0.0824 s of solution time was taken whereas only 0.0518s were needed for the 8mm oil injection port. A similar check was made for the discharge pressure of 10.5bar.

Figure 2b shows that the oil flow rate increases linearly with the oil port diameter for both cases. The final mass imbalance for the air phase had an average value of 0.57% at 8.5bar and 0.30% at 10.5bar, while for the oil phase it was 4% at 8.5bar and 2.3% at 10.5bar.
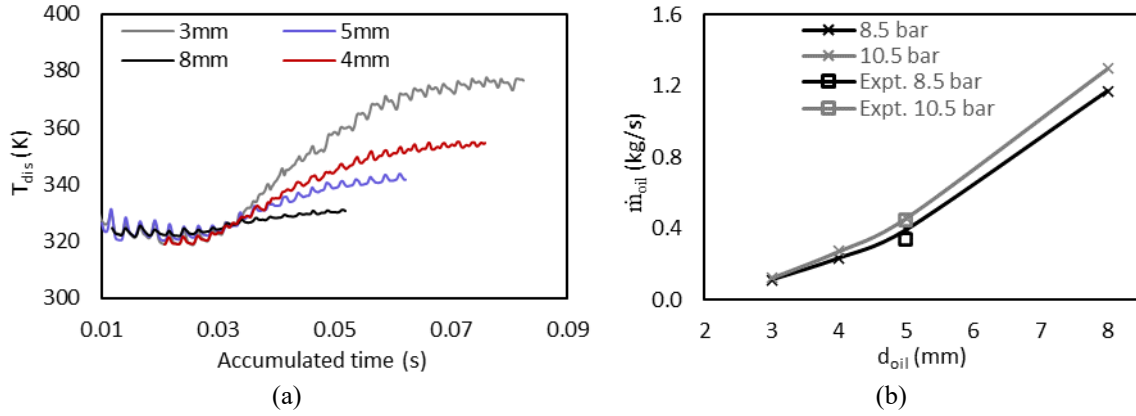

Figure 2. (a) Discharge temperature at 8.5bar and (b) Averaged oil flow rate for different oil injection port diameter at 8.5 and 10.5bar

3. EXPERIMENTAL SETUP

The screw compressor used in this study (Table 1) is measured in the test rig installed at City, University of London to determine the air flow rate, compressor power, specific power, adiabatic and volumetric efficiency. The photograph of the test rig and the instrumentation diagram is shown in Figure 3. Measurements are performed according to ISO 1217:2009. The air flow rate was measured by means of an orifice plate, according to BS 5600. The compressor inlet and outlet temperatures were measured by Platinum Resistance Thermometers with errors within ±0.50 °C. Oil temperatures were measured by K-type thermocouples with errors within ± 1.0 °C. All pressures were measured with transducers with errors within ± 0.6%. The compressor speed was measured by a shaft encoder with ±2.7% error. The compressor torque was measured by the torque meter with a strain gauge transducer with the accuracy of ±0.25%. All tests were carried out at the rotational speed of 6000 rpm.

P, T, T_{ql}, and S are the pressure, temperature, torque and speed measurement points in the test rig. CompactRIO (CRIO-9022) system and Labview software were used for data acquisition and calculation of the performance. Up to 20 readings of dynamic data were collected every 10s and averaged to eliminate any measurement noise. Measured pressures, air flow rate, shaft torque, rotational speed are substituted in equations (8)-(12) to obtain compressor performance parameters of power, adiabatic efficiency, volumetric efficiency and specific power. The value of theoretical air flow rate, for the compressor in this study, is 4.35 m³/min.

$$PW_{ad} = \frac{\gamma}{\gamma - 1} P_1 . 60. Q_v. \left[\left(\frac{P_2}{P_1} \right)^{\frac{\gamma-1}{\gamma}} - 1 \right] \tag{8}$$

$$PW_{comp} = \frac{\tau N}{60} \tag{9}$$

$$\eta_{ad} = PW_{ad}/PW_{comp} \tag{10}$$

$$\eta_v = Q_v/Q_{th} \tag{11}$$

$$w_{comp} = PW_{comp}/Q_v \tag{12}$$

The error analysis was performed according to [31] and [32]. It resulted in the following accuracy: air flow rate 3.7%, power input, 2.7%, specific power 5.5%, and oil flow 12.8%. The performance obtained for the tested compressor are shown in Table 8.
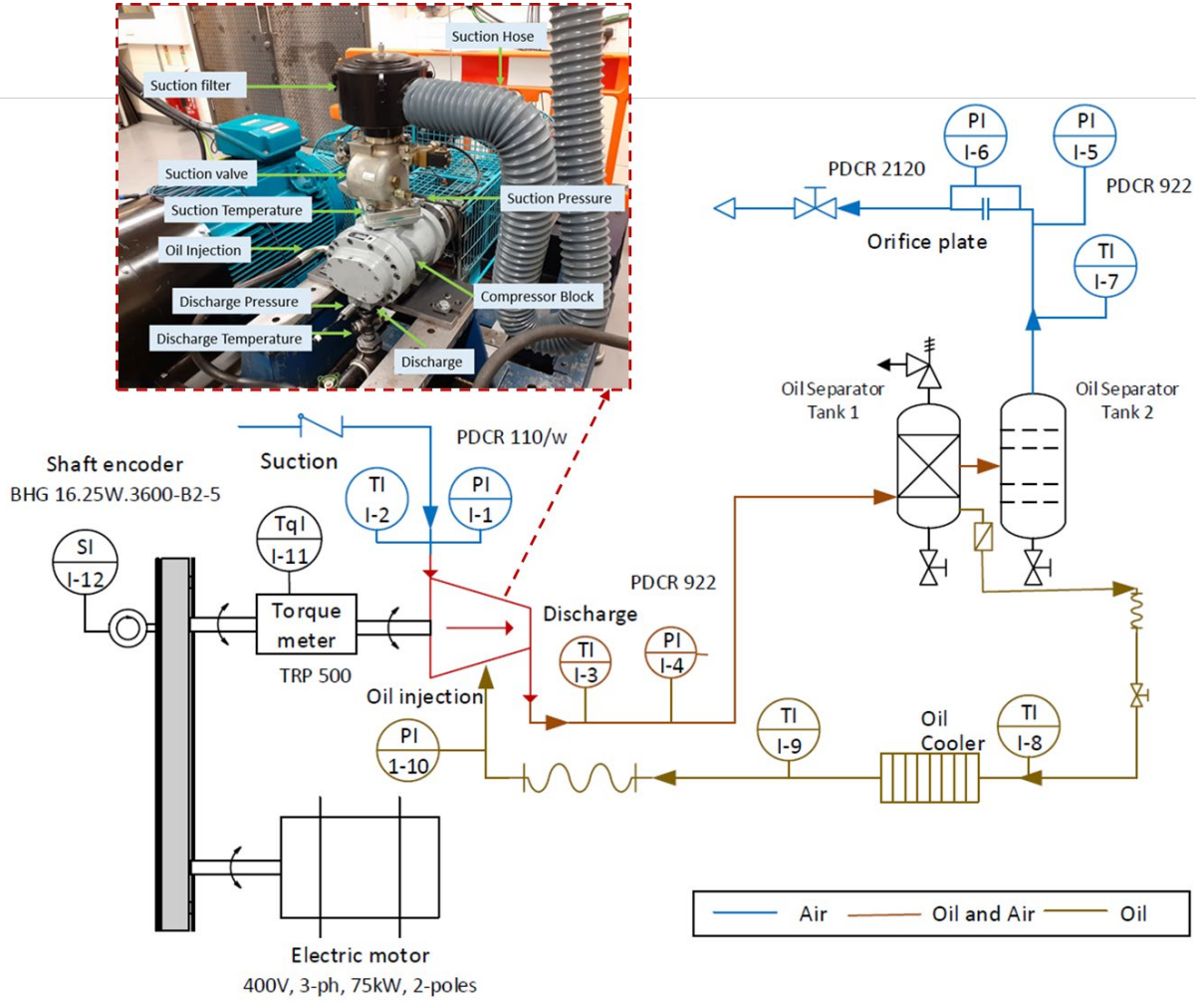
Figure 3. Layout and instrumentation of the compressor test rig

Table 8. Test results obtained for a single oil injection port diameter of 5mm

Pressure ratio P_2/P_1	Power PW [kW]	Volume flow rate Q_v [m³/min]	Volumetric efficiency η_v [%]	Adiabatic efficiency η_{ad} [%]	Specific Power w_{comp} [kW/m³/min]
8.5	24.4	3.73	85.6	75.3	6.53
10.5	27.0	3.67	84.2	76.0	7.35

4. RESULTS AND DISCUSSIONS

A total of ten cases at different oil injection conditions and two different pressure ratios are calculated. The distribution of oil and temperature field in the cells near the rotor surface are illustrated and quantified in this section. Moreover, the performance parameters of power, air flow rate, volumetric efficiency, adiabatic efficiency, and specific power are recorded and compared between the calculated case studies and experimental data.

4.1 Oil injection through the single injection port.

4.1.1 Oil and temperature distribution

Figure 4 shows the visualisation of the oil distribution in the compression domain using the VOF model at P_{out}=8.5 bar and the male rotor speed of 6000 rpm.

(a) d_{oil}= 3mm and $\dot{m}_{oil}$= 0.11 kg/s, t= 0.0805s   (b) d_{oil}= 4mm and $\dot{m}_{oil}$= 0.23 kg/s, t= 0.0733s

(c) d_{oil}= 5mm and $\dot{m}_{oil}$= 0.39 kg/s, t= 0.0733s   (d) d_{oil}= 8mm and $\dot{m}_{oil}$= 1.17 kg/s, t=0.0505s
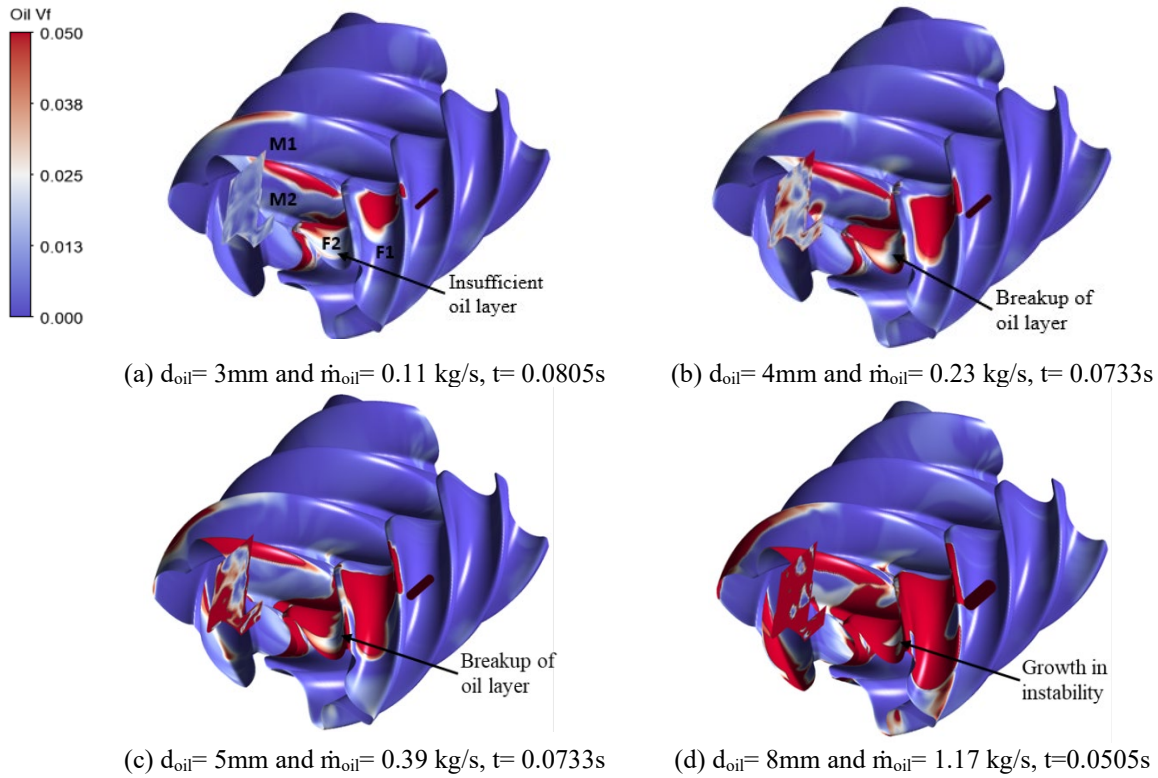
Figure 4. Oil volume fraction in the first layer of cells adjacent to rotors at 6000 RPM and 8.5bar discharge pressure

The oil distribution shown by the oil volume fraction and the gas temperature in the first layer of numerical fluid cells adjacent to the rotor surface are shown in Figure 4 a-d and Figure 6a-d, respectively. As shown in Figure 4a and 6a, the 3mm nozzle does not supply sufficient oil and the gas temperature locally reaches up to 220°C. At the same time, as shown in Figure 5, the discharge temperature exceeds 110°C. Figure 4b and Figure 4c show the spreading of the oil layer further on the female rotor surface with the oil nozzles of 4mm and 5mm. With the rotation of rotors, this layer shears and breaks, and it will reach the axial discharge clearance on the female rotor side. However, it could be observed that it does not spread on the male rotor as widely as on the female rotor. The discharge temperature is below 90°C for both cases, as shown in Figure 5. For the 4mm oil injection hole, the local gas temperature on the female rotor leading tip exceeds 100°C while for the 5mm oil injection, the female rotor side is well cooled. However, in both cases, the male rotor side experiences hot zones above 100°C with temperatures in some regions as high as 189°C for 4mm nozzle and around 157°C for 5mm nozzle.
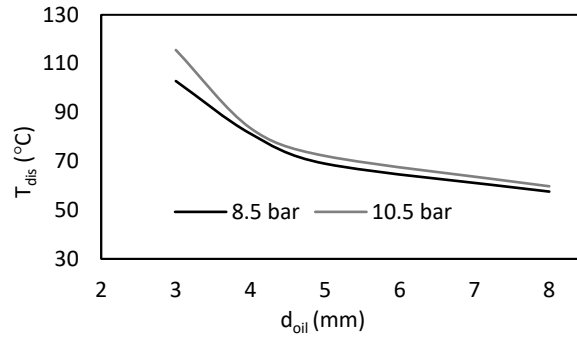
Figure 5. Discharge temperature as a function of the oil port diameter at 6000 rpm, 8.5 and 10.5bar discharge pressure

Further increase in the diameter of this single injection port will increase the oil flow in the compressor. Thus, changing the orifice from 5mm to 8mm increases the oil flow by a factor of 2.8, but results in the gas temperature reduction of only 11°C. The excess of oil does not contribute sufficiently to the cooling of the gas. The large oil content results in a very stable oil layer, as shown in Figure 4d. An important point to note is that, even with this highest oil mass flow rate of 1.17kg/s, the distribution of oil on the male rotor side remains sparse and the temperature still exceeds 100°C in certain regions.

It can be concluded that, with the single oil injection port on the female rotor side, the oil layer sufficiently spreads on the female rotor side, but the oil does not spread effectively on the male rotor. Hence, the increase in the oil flow rate helps to reduce the gas discharge temperature, which drops down to 50°C but the local temperature inside the domain on the male rotor side remains above 100°C. Moreover, the excessive amount of oil requires larger equipment in the compressor system and adversely affects the total efficiency of the compressor, and therefore it is not recommended as a method for optimisation of compressors.

(a) d_{oil}= 3mm and $\dot{m}_{oil}$= 0.11 kg/s, t= 0.0805s   (b) d_{oil}= 4mm and $\dot{m}_{oil}$= 0.23 kg/s, t= 0.0733s

(c) d_{oil}= 5mm and $\dot{m}_{oil}$= 0.39 kg/s, t= 0.0733s   (d) d_{oil}= 8mm and $\dot{m}_{oil}$= 1.17 kg/s, t=0.0505s
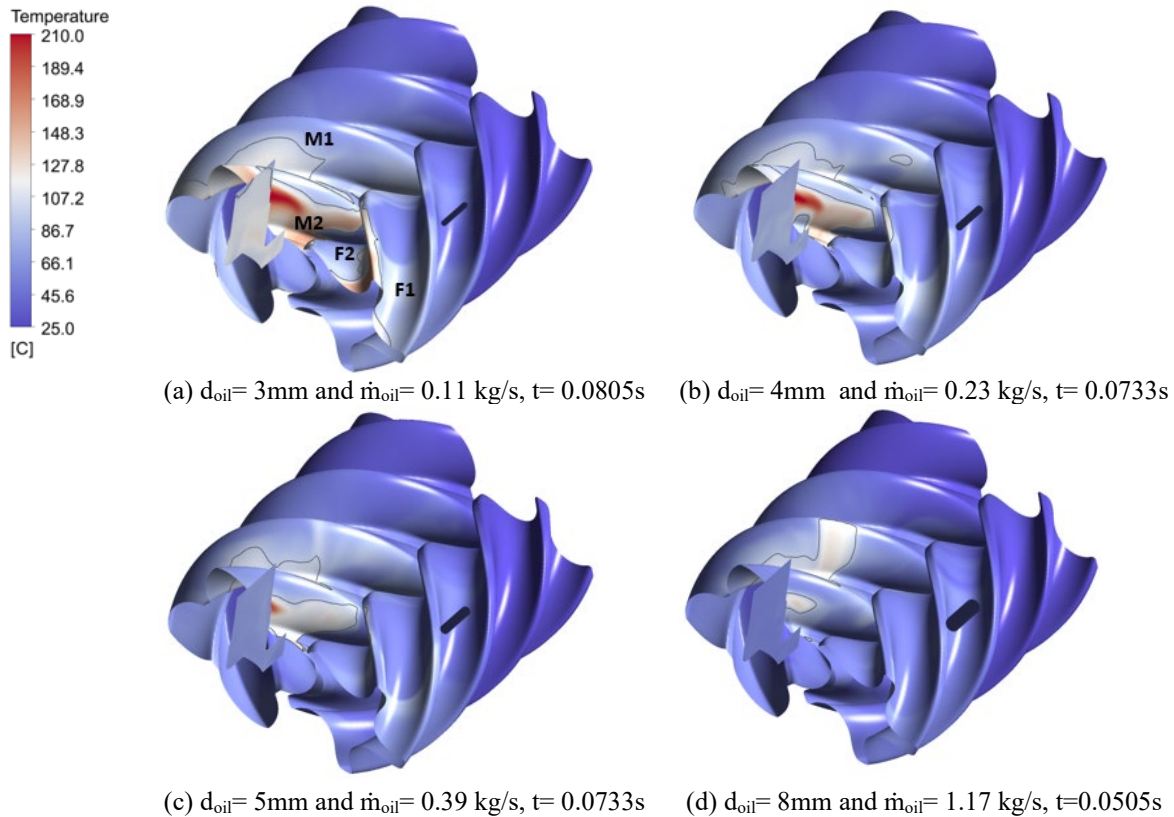
Figure 6. Local gas temperature in the first layer of cells adjacent to rotors at 6000 RPM and 8.5bar discharge pressure
The regions bounded by the isolines represent areas where temperatures exceed 100°C

Bar plots shown in Figure 7 represent the oil volume fraction and temperature versus the percentage of rotor surface areas where these values apply. Majority of the rotor surface area is covered with very low oil volume fraction between 0.0-0.1 and therefore not included in the figure. The same applies the surfaces areas with low temperatures. Value of the oil volume fraction and temperature is from the cells near the rotor surface.

The total surface area of the male rotor is 70,947mm^2, and for the female rotor, it is 58,263mm^2.
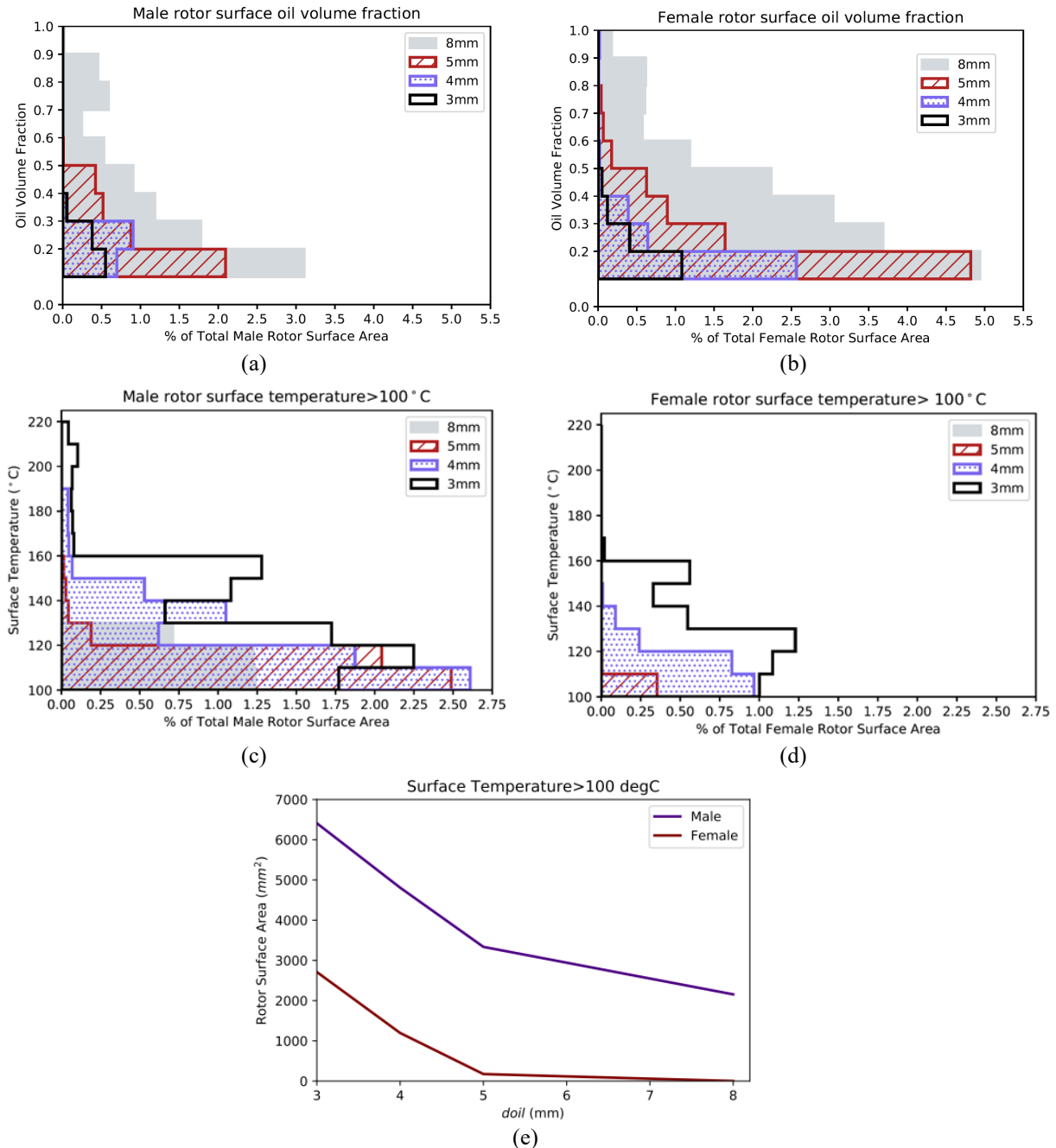

(a)

(b)

(c)

(d)

(e)

Figure 7. Distribution of oil and temperatures of air on the male and female rotors shown as the percentage of the rotor surface.

Changing the oil injection port diameter from 3mm to 8mm increases the mass flow rate of oil 9.5 times, but the total surface area wetted by oil increases only 5.5 times. Moreover, by injecting oil through a single injection point on the female rotor side, the oil flooded female rotor surface is 1.7 times higher than the oil flooded male rotor surface. This

disparity between the male and female rotor sides is shown in Figure 7a and Figure 7b. This results in fluid temperatures beyond 100°C to cover much larger rotor surface areas on the male rotor than on the female, as shown in Figure 7c and Figure 7d. It is important to notice here that the percentage of the rotor surface area in contact with oil is relatively small compared to the total rotor surface, which is also visible in previous figures.

To appreciate the significance of the surface temperatures close to rotors, the total surface areas with temperatures higher than 100°C, are summed up for various oil injection diameters in Figure 7e, where a large difference between the surface areas with high temperatures on the male and female rotors can be observed, thus emphasising the need for better distribution of the oil to transfer the heat more evenly.

4.1.2 *Effect on the compressor performance*

The comparison between the performance predicted from CFD calculations and the performance measured in the test rig is shown in Figure 8a-e. The difference for the air flow rate is 0.5% at 8.5bar and 0.7% at 10.5bar while the difference for power is around 3.0% at 8.5bar and 2.3% at 10.5bar. This upholds the confidence in the reliability of CFD predictions.
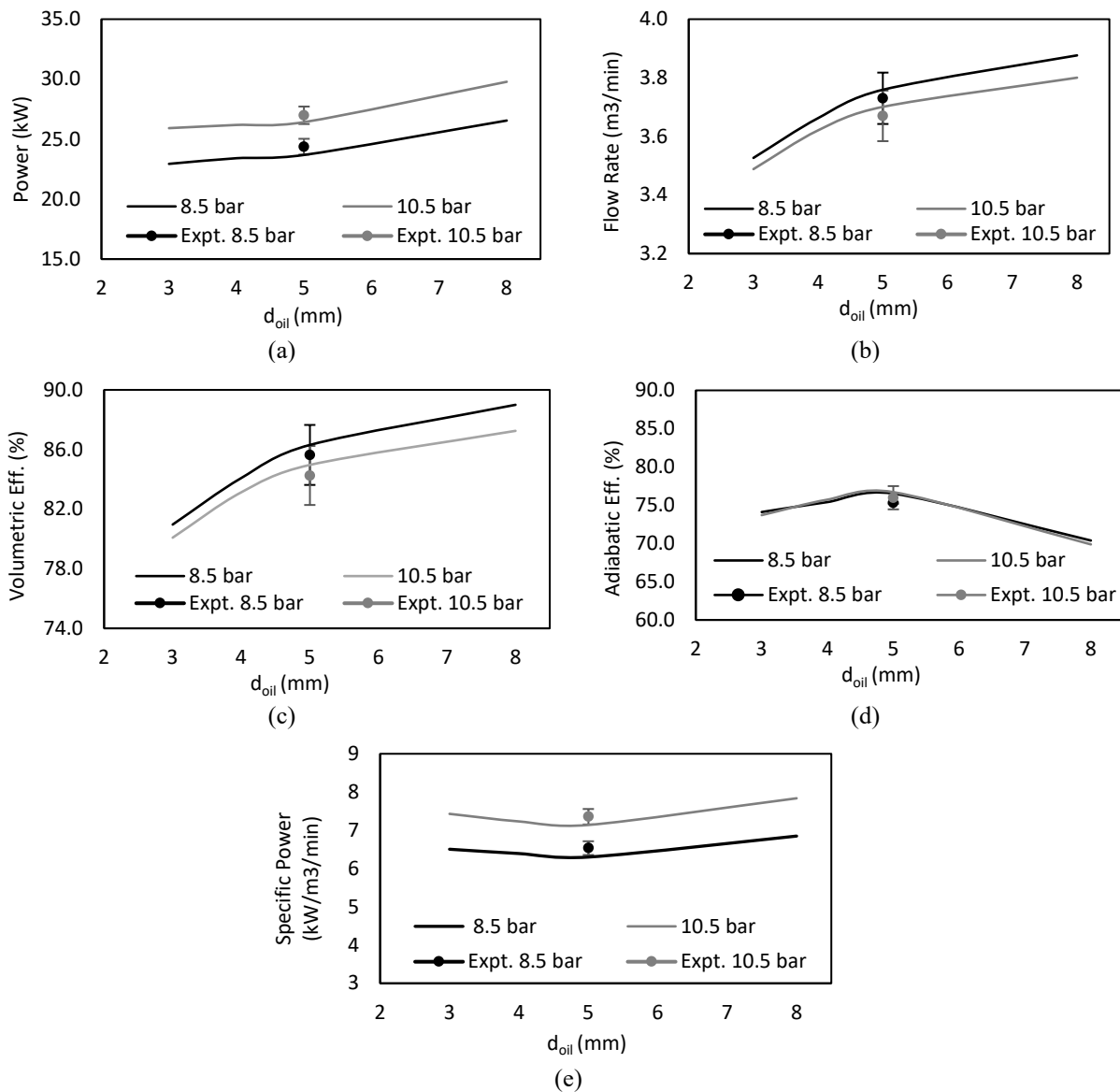

Figure 8. (a) power, (b) air flow rate, (c) volumetric efficiency, (d) adiabatic efficiency and (e) specific power and with oil port diameter for discharge pressure of 8.5bar and 10.5bar

Based on these predictions and measurements, the next section presents the investigation on improvements in rotor cooling and specific power using a separate injection port on each rotor side.

4.2   Oil injection through two injection ports

The CFD analysis of this oil-injected screw compressor with oil injection through the single port showed the uneven distribution of oil on the female and male rotors that caused the excessive gas temperature in the male rotor domain. It was suggested that design alterations are required to reduce the internal gas temperature. An additional oil injection port was added in the casing on the male rotor side to resolve this. The cumulative oil flow rate from the two injection ports is made equal to the optimum oil flow rate calculated for the single injection port, and the port is positioned to match the injection angle similar to the female rotor.

The single-port oil injection selected for this comparative study had a diameter of 5mm with an oil flow rate of 0.39kg/s and 0.46kg/s at 8.5bar and 10.5bar compressor discharge pressures, respectively. The diameters of both injection ports were 3.6mm for the female rotor and 3.5mm for the male rotor. This resulted in a total oil flow rate from both ports being 0.35kg/s, and 0.41kg/s at 8.5bar and 10.5bar, respectively. This, on average, resulted in a 9.7% lower total flow rate. The calculated oil flow rates are shown in Table 7. Better matching could not be achieved because the second decimal accuracy would be required in the sizing of orifices, and this would be impractical to manufacture. Also, each nozzle's pressure difference would not be the same due to the difference in their positioning.

4.2.1   Oil distribution and temperatures for two-point oil injection

The CFD calculation results for the single injection port and two injection ports are presented in Figure 9 showing the oil distribution, and in Figure 10 the temperature of the fluid next to the compressor rotors. Both are at the discharge pressure of 8.5bar and the male rotor rotational angle of 30°.
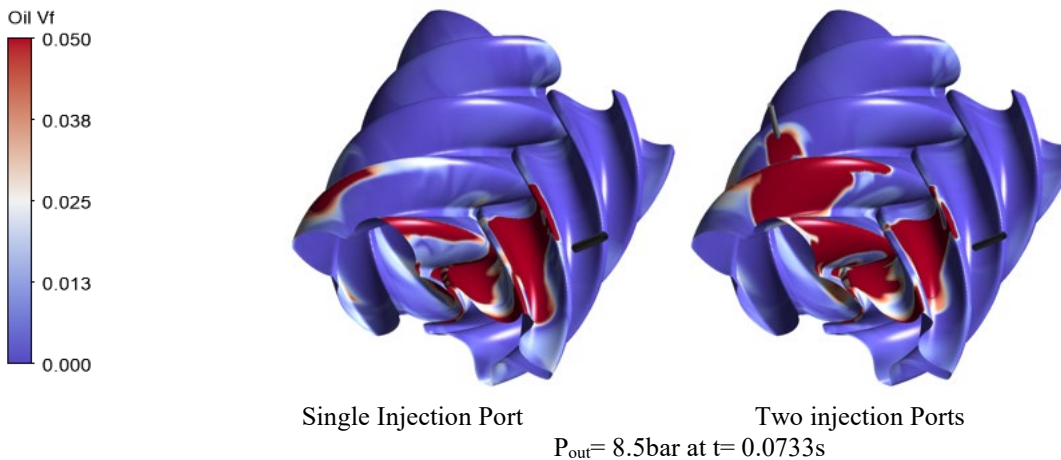

Single Injection Port   Two injection Ports
P_{out}= 8.5bar at t= 0.0733s

Figure 9. Comparison of oil distribution for the single injection port and the two injection port Video link: https://drive.google.com/file/d/1W5Gz_lEhnqDvRcQ5pKVuJUrWmYpvIatC/view?usp=sharing

Looking at the left Figure 9 where oil is injected through the single port, most oil flow is directed towards the outlet through the working domain associated with the female rotor. Some oil is directed towards the male rotor tips due to inertial forces. This is beneficial for sealing the radial clearance gaps, but the amount of oil in the working chamber is very low. This poor oil distribution results in high temperatures of air between the male rotor lobes. Figure 10 shows that the temperature in this region well exceeds 100°C reaching up to 157°C.

By injecting oil through two injection ports, one on the male and another on the female rotor the distribution of oil in the working chamber on the male rotor side improved significantly. As shown in Figure 10, the area in which the temperature exceeds 100°C is significantly reduced, and the maximum temperature is reduced to 127°C.
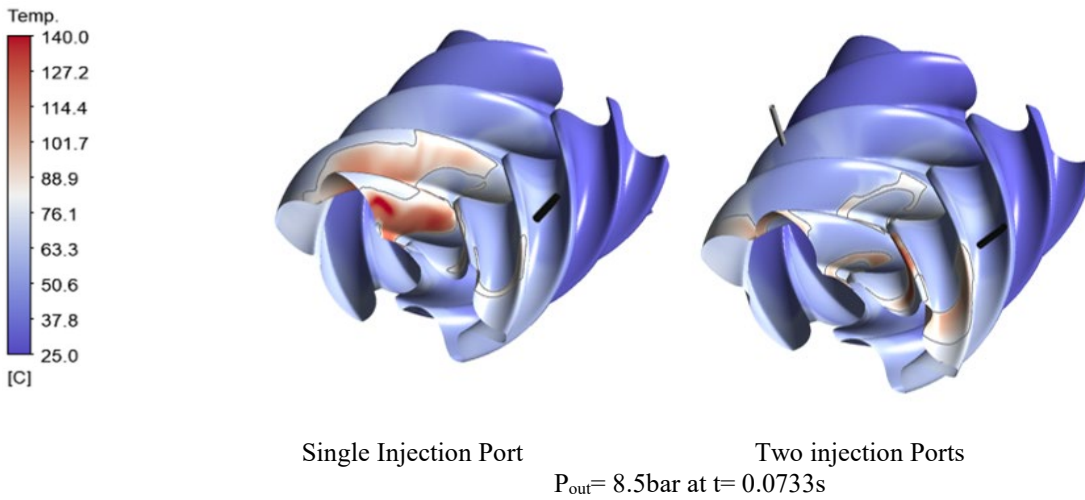
Single Injection Port   Two injection Ports

P_{out}= 8.5bar at t= 0.0733s

Figure 10. Comparison of the gas temperatures for the single injection port and the two injection port . Video link: https://drive.google.com/file/d/163uTiRWc7FLQRCH4QnfOhiwPavmN0esb/view?usp=sharing

To further appreciate the differences in oil distribution between the single oil injection port and two injection ports, plots for the oil volume distribution on rotor surfaces are shown in Figure 11a and Figure 11b. Here the rotor surface area is the surface area of the cells containing certain values of oil volume fraction and temperatures. These bar plots show that separate injection to each rotor clearly reduces the wetted female rotor region area and supplements an increase in the wetted area near the male rotor region. It can be seen from Figure 12 that the use of two injection ports drastically alters the local temperatures. Both are at the discharge pressure of 8.5bar.

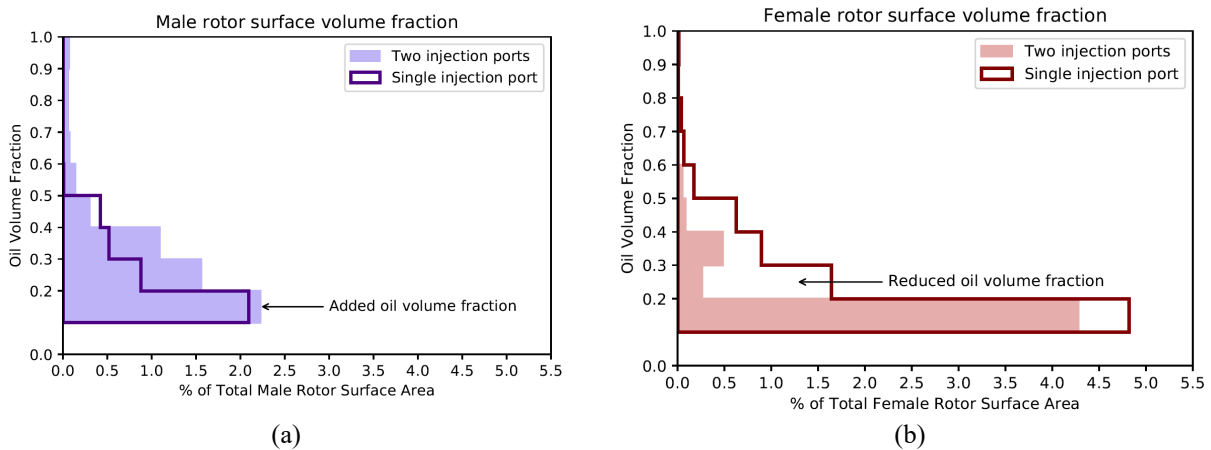(a)   (b)

Figure 11. Rotor surface area with (a) oil volume fraction on the male rotor for 8.5 discharge pressure and (b) oil volume fraction on the female rotor for 8.5bar discharge pressure

To improve visualisation, rotor surface areas are shown for face temperatures beyond 90°C at 8.5bar and 10.5bar in Figure12a and Figure12b. The percentage of rotor surface areas with high temperatures on the male rotor is significantly reduced with the two injection ports.
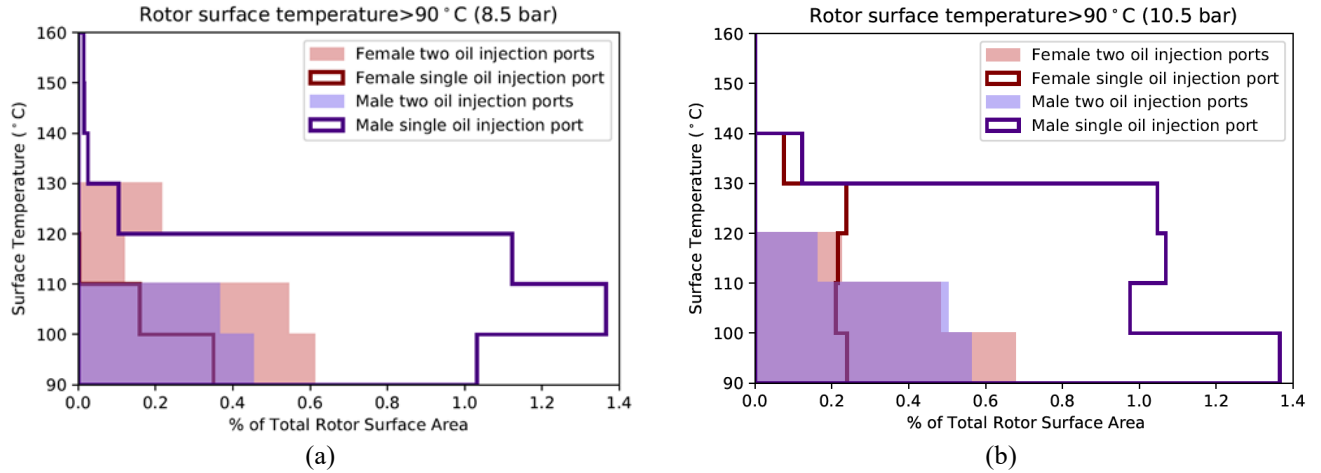
Figure 12. Rotor surface area with surface temperatures over 90°C on both rotors (a) at 8.5bar, (b) at 10.5bar

As shown in Table 9, the oil injection through two ports led to the reduction in maximum temperatures of 30 °C at 8.5bar and 35 °C at 10.5bar

Table 9. Maximum temperature reduction with single and dual ports

Injection Type	T_{max} [°C]	
	P_{out}: 8.5bar	P_{out}: 10.5bar
Single injection port	157	150
Two injection ports	127	115
ΔT	30	35

4.2.2   Effect on the compressor performance

Performance improvements due to the use of two oil injection ports are shown in Figure 13. The addition of the second port did not influence the air flow rate. At the same time, the oil flow rate was reduced by 9%. The main effect on the performance was by reduction in power consumption for the two injection ports. Indicated power reduced by 2.1% and 1.8% for 8.5bar and 10.5bar discharge pressure, respectively. This combined effect of flow and power reduced specific power by around 1.8% for both 8.5and 10.5bar discharge pressures.
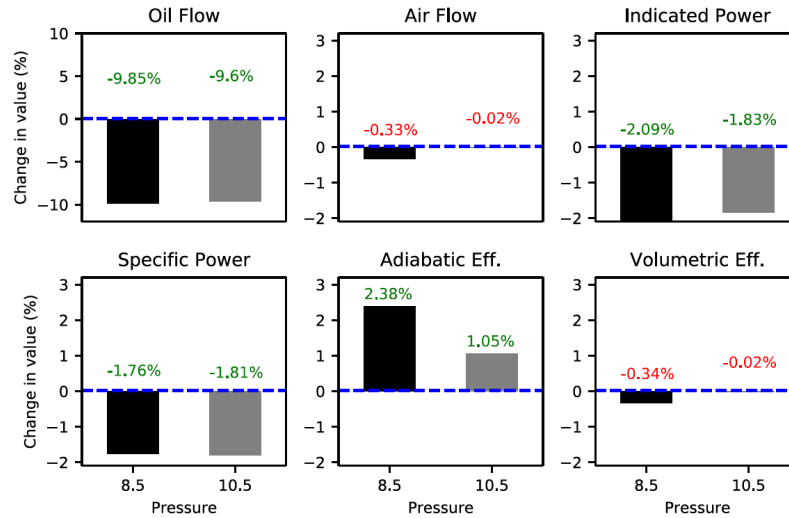
Figure 13. Comparison of the two injection ports and the single oil-injection port configurations at discharge pressures of 8.5 and 10.5bar. The green coloured text indicates improvement levels with the two port configuration.

5. CONCLUSIONS

CFD analysis of the fluid flow, and temperature distribution within the oil injected twin screw air compressor, with the VOF multiphase model was used to evaluate improvements, by introducing two-point oil injection. This was carried out for a compressor with the 4/5 lobe combination, operating at the male rotor shaft speed of 6000 RPM at discharge pressures of 8.5 and 10.5bar. The predicted results of the single injection port were compared with results obtained by measuring this compressor. Both power and flow predictions were close to experimental results with differences of 0.5% for flow and 3% for power, respectively, at 8.5bar and 0.7% for flow and 2.3% for power at 10.5bar.

The model was used to evaluate oil and temperature distribution and performance of the compressor with the single oil injection port located in the casing close to the female rotor, and with the two injection ports injecting to both male and female rotors. The total injection flow was retained in both cases by adjusting the size of the oil injection ports. The key conclusions from this study are:

- This computational procedure produced results in a good agreement with measurements.
- This analysis method enabled both the oil and temperature distribution to be evaluated within the compression chamber and to visualise how the oil layer was formed and broke up close to the rotor surfaces.
- It was concluded that the temperature of the gas at rotor surfaces was determined by the oil distribution and that hot spots were found to coincide with regions where oil concentration was low.
- By increasing the orifice diameter of the single injection port, it was possible to reduce the air discharge temperature but, despite this, it was found out that there was an optimum value for the oil injection rate, beyond which there was no significant gain in the cooling of the gas.
- With a single oil injection hole on the female side, the temperature in the compression chamber on the male rotor reached 157°C at some rotor points, although temperatures on the female rotor side were far lower. It was therefore decided to determine whether the maximum surface temperatures could be reduced by oil injection into both the male and female rotor sides of the casing.
- The study showed that with two injection ports and the same total oil injection flow rate, the predicted indicated power was reduced by 2.1% and 1.8% at 8.5bar and 10.5bar, respectively. The specific power was reduced by 1.8% in both cases, while the maximum internal temperature with the oil injection holes on both rotor sides was reduced to 127°C, which was an improvement of 30-35ºC.

Author Contributions
Nausheen Basha: Investigation, Writing- Original draft preparation. Conceptualisation, Methodology, Software, Investigation **Ahmed Kovacevic:** Conceptualisation, Writing- Reviewing and Editing, Supervision **Sham Rane**: Software

REFERENCES

[1]   Compressed air equipment presentation by Department for Business, Energy and Industrial Strategy, 2020. https://assets.publishing.service.gov.uk/government/uploads/system/uploads/attachment_data/file/879754/C ompressed_Air_Technology_Information_Leaflet_-_April_2020.pdf (accessed Oct. 03, 2020).

[2]   S. Abdan, N. Basha, A. Kovacevic, N. Stosic, A. Birari, and N. Asati
        Development and Design of Energy Efficient Oil-Flooded Screw Compressors
        IOP Conference Series: Materials Science and Engineering, 604 (2019), pp. 1, doi: 10.1088/1757-899X/604/1/012015.

[3]   P. Singh and J. Bowman
        Heat Transfer in Oil-Flooded Screw Compressors
        Int. Compress. Eng. Conf., (1986), pp. 135–153.

[4]   N. Stošic, L. Milutinović, K. Hanjalić, and A. Kovačević
        Investigation of the influence of oil injection upon the screw compressor working process
        Int. J. Refrig., 15 (1992), no. 4, pp. 206–220, doi: 10.1016/0140-7007(92)90051-U.

[5]   X. Peng, Z. Xing, T. Cui, and P. Shu
        Experimental Study of Oil Injection and Its Effect On Performance of Twin Screw Compressors
        Int. Compress. Eng. Conf., (2000).

[6]   M. De Paepe, W. Bogaert, and D. Mertens
        Cooling of oil injected screw compressors by oil atomisation
        Appl. Therm. Eng., 25 (2005), pp. 2764–2779, doi: 10.1016/j.applthermaleng.2005.02.003.

[7]   A. Kovacevic
        Boundary adaptation in grid generation for CFD analysis of screw compressors
        Int. J. Numer. Methods Eng., 64(2005), no. 3, pp. 401–426, doi: 10.1002/nme.1376.

[8]   A. Kovacevic and S. Rane
        Algebraic generation of single domain computational grid for twin screw machines Part II – Validation
        Adv. Eng. Softw., (2017). doi: 10.1016/j.advengsoft.2017.03.001.

[9]   N. Casari, E. Fadiga, M. Pinelli, S. Randi, A. Suman, and D. Ziviani
        Investigation of flow characteristics in a single screw expander: A numerical approach
        Energy, 213 (2020), p. 118730, doi: 10.1016/j.energy.2020.118730.

[10]   S. Rane, A. Kovacevic, and N. Stosic
        CFD Analysis of Oil Flooded Twin Screw Compressors
        Int. Compress. Eng. Conf., (2016).

[11]   I. Papes, J. Degroote, and J. Vierendeels
        Development of a thermodynamic low order model for a twin screw expander with emphasis on pulsations in the inlet pipe
        Appl. Therm. Eng., 103(2016), pp. 909–919, doi: 10.1016/j.applthermaleng.2016.04.159.

[12]   I. Papes, J. Degroote, and J. Vierendeels
        New insights in twin screw expander performance for small scale ORC systems from 3D CFD analysis
        Appl. Therm. Eng., 91 (2015), pp. 535–546, doi: 10.1016/j.applthermaleng.2015.08.034.

[13]   H. Ding and Y. Jiang
        CFD simulation of a screw compressor with oil injection
        10th International Conference on Compressors and their Systems, (2017).

[14]   ANSYS Fluent User's Guide, 2019R1, 2019.

[15]   N. Basha, S. Rane, and A. Kovacevic
        Multiphase Flow Analysis in Oil-injected Twin Screw Compressor
        3rd World Congress on Momentum, Heat and Mass Transfer, (2018), doi: 10.11159/icmfht18.132

[16]   N. Basha, A. Kovacevic, and S. Rane
        Analysis of Oil-Injected Twin-Screw Compressor with Multiphase Flow Models
        Designs, 3 (2019), no. 4, p. 54, doi: 10.3390/designs3040054.

[17]   W. Wu, C. Hu, J. Hu, and S. Yuan
        Jet cooling for rolling bearings: Flow visualization and temperature distribution
        Appl. Therm. Eng., 105 (2016), pp. 217–224, doi: 10.1016/j.applthermaleng.2016.05.147.

[18]   W. Wu, C. Hu, J. Hu, S. Yuan, and R. Zhang
        Jet cooling characteristics for ball bearings using the VOF multiphase model
        Int. J. Therm. Sci., 116(2017), pp. 150–158, doi: 10.1016/j.ijthermalsci.2017.02.014.

[19]   J. Wu and G. Wang
        Numerical study on oil supply system of a rotary compressor
        Appl. Therm. Eng., 61 (2013), no. 2, pp. 425–432, doi: 10.1016/j.applthermaleng.2013.07.047.

[20]   C. W. Hirt and B. D. Nichols
        Volume of Fluid (VOF) Method for the Dynamics of Free Boundaries
        Journal of Computational Physics, 225(1981), pp. 201–225, doi: 10.1016/0021-9991(81)90145-5

[21]   M. Wörner
        Numerical modeling of multiphase flows in microfluidics and micro process engineering: A review of methods
        and applications
        Microfluidics and Nanofluidics, (2012), doi: 10.1007/s10404-012-0940-8.

[22]   ANSYS FLUENT theory guide- Release 19.0, ANSYS, Inc. 2018, doi: 10.1016/0140-3664(87)90311-2.

[23]   SCORG Help Manual- Release 5.7. London, UK: PDM Analysis Limited, 2019.

[24]   A. Kovacevic, N. Stosic, and I. Smith,
        Screw Compressors Three Dimensional Computational Fluid Dynamics and Solid Fluid Interaction, Springer,
        2007.

[25]   S. Rane and A. Kovacevic
        Algebraic generation of single domain computational grid for twin screw machines . Part I . Implementation
        Adv. Eng. Softw., 107 (2017), pp. 38–50, doi: 10.1016/j.advengsoft.2017.02.003.

[26]   A. Kovacevic
        Three-Dimensional Numerical Analysis for Flow Prediction in Positive Displacement Screw Machines, City
        University London, (2002).

[27]   G. Bianchi, S. Rane, A. Kovacevic, and R. Cipollone
        Deforming grid generation for numerical simulations of fluid dynamics in sliding vane rotary machines
        Adv. Eng. Softw., 112 (2017), pp. 180–191, doi: 10.1016/j.advengsoft.2017.05.010.

[28]   N. Basha, A. Kovacevic, and S. Rane
        User defined nodal displacement of numerical mesh for analysis of screw machines in FLUENT
        IOP Conference Series: Materials Science and Engineering, 604 (2019), pp. 012012, doi: 10.1088/1757-
        899X/604/1/012012.

[29]   Y. Lu, A. Kovacevic, M. Read, and N. Basha
        Numerical Study of Customised Mesh for Twin Screw Vacuum Pumps
        Designs, 3(2019), no. 4, pp. 1–18, 2019, doi: 10.3390/designs3040052.

[30]   ANSYS Meshing User's Guide-Release 13.0. Canonsburg, PA 15317: Ansys Inc., 2010.

[31]   A Summary of Error Propagation, Harvard University, 2013. http://ipl.physics.harvard.edu/wp-
        uploads/2013/03/PS3_Error_Propagation_sp13.pdf (accessed May 09, 2018).

[32]   N. Basha, A. Kovacevic, N. Stosic, and I. Smith
        Effect of oil-injection on twin screw compressor performance
        IOP Conf. Ser. Mater. Sci. Eng., (2018), doi: 10.1088/1757-899X/425/1/012009.